Angewandte Chemie International Edition

Angewandte International Edition Chemie

How to cite: *Angew. Chem. Int. Ed.* **2026**, e7355159
doi.org/10.1002/anie.7355159

RESEARCH ARTICLE

Dynamic Covalent Se—Se Bonds Enable Mechanically Adaptive Selenium Crystals

Chaowei He[1] | Wenjie Zhang[1] | Ruihao Zhou[1] | Zeyu Lu[1] | Zhigang Shuai[2] | Huaping Xu[1]

[1]Key Laboratory of Bioorganic Phosphorus Chemistry & Chemical Biology, Department of Chemistry, Tsinghua University, Beijing, China | [2]School of Science and Engineering, The Chinese University of Hong Kong, Shenzhen, Guangdong, China

Correspondence: Huaping Xu (xuhuaping@mail.tsinghua.edu.cn)

Received: 23 March 2026 | **Revised:** 4 May 2026 | **Accepted:** 7 May 2026

Keywords: diselenide bonds | dynamic covalent chemistry | dynamic polymer | dynamic crystal | stimuli-responsiveness

ABSTRACT

Dynamic covalent chemistry has enabled adaptive behavior in organic polymer networks and molecular crystals, yet analogous control in inorganic crystalline solids remains largely unexplored. Here we show that elemental selenium can operate as a dynamic covalent inorganic crystal, whose architectural and functional adaptability arises from dynamic covalent Se—Se bonds within the trigonal selenium backbone. External mechanical (or optical) stimuli drive Se—Se bond cleavage and reformation, mediating structural reconfiguration of the crystalline framework. Embedding selenium in a crosslinked polymer matrix creates a mechanically programmable environment that exerts real-time and persistent mechanical signals in situ. Under this chemo-mechanical coupling, crystal branching frequency and three-dimensional architecture respond to matrix stiffness and external light, and these translate directly into tunable dielectric behavior in polymer-selenium composites. This work expands dynamic covalent chemistry from organic to inorganic crystalline materials, and reveals dynamic covalent inorganic crystals as a new class of adaptive materials.

1 | Introduction

Crystals, particularly inorganic crystals, are conventionally viewed as rigid and static solids, whereas adaptability and stimulus responsiveness are defining hallmarks of soft matter [1–4]. Bridging gap of these two regimes by endowing crystals with intrinsic dynamicity, represents a conceptual beyond traditional views and a fundamental challenge in intelligent materials science [5–10].

Toward this goal, dynamic covalent chemistry, widely exploited in polymers for switchable chemical bond and network reconfiguration [11–16], has been introduced into organic molecular crystals, enabling transformation of the constituent units [17–20] and collective, responsive behaviors [21–25]. However, such dynamic behavior is far less explored in inorganic crystals, due to strong atomic bonding and three-dimensional lattice connectivity that generally suppress bond dynamics and structural plasticity. Extending the concept of dynamic covalent chemistry to inorganic crystals is therefore both scientifically challenging and appealing, as it would expand the materials landscape for responsive and adaptive functionalities.

Elemental selenium offers a compelling opportunity to address this challenge [26, 27]. Its trigonal crystal consists of an inorganic dynamic covalent backbone, Se_n, where one-dimensional helical chains linked by Se—Se bonds [28, 29]. Se—Se bonds have relatively low bond energies (172 kJ/mol) [30, 31] and represent

Chaowei He and Wenjie Zhang contributed equally to this work.

a typical class of dynamic covalent bonds capable of reversible cleavage and reformation under multiple stimuli, including light, heat, and mechanical force [32–36]. These characteristics increase susceptibility of crystal framework to structural perturbation [37–41], suggesting that selenium crystals may possess an intrinsic capacity for dynamic structural response as a "dynamic polymer" [30], despite their inorganic composition. However, whether such bond-level dynamicity can be activated within a crystalline lattice and translated into adaptive crystal behavior and property modulation has not been demonstrated.

Here, we show that selenium crystals can exhibit structural and functional adaptivity through stimuli-induced cleavage and reformation of dynamic covalent Se—Se bonds. We develop an in situ reaction-induced crystallization strategy that generates elemental selenium directly within a crosslinked polymer network (PSe_xG_y), thereby integrating a dynamic covalent inorganic backbone into a mechanically programmable soft matrix. In this composite architecture, the polymer network acts as a tunable mechanical environment that delivers persistent, spatially heterogeneous stress fields to the selenium while maintaining continuous and intimate interfacial contact. Under this chemo-mechanical coupling, the Se—Se bond exchange within the trigonal selenium backbone enables local stress relaxation and defect formation, which are expressed at the macroscale as mechanically regulated branching frequency and three-dimensional crystal architecture. Beyond the structural adaptivity, these mechanically regulated morphologies, in turn, translate directly into tunable dielectric behavior in polymer-selenium composites. More broadly, our results establish that dynamic covalent bond exchange can endow inorganic crystals with architectural and functional adaptability, expanding dynamic covalent chemistry from organic polymer networks and molecular crystals to inorganic crystalline solids.

2 | Results and Discussion

2.1 | In Situ Formation of Selenium Crystals in Polymer Networks

The in situ growth of selenium crystal within polymer matrix was achieved through a strategy of "reaction induced crystallization", which employed a selenium-containing polymer as a precursor, followed by a photochemical reaction to generate elemental selenium below the melting point, leading to crystallization (Figure 1a). This approach circumvents the poor thermal stability of polymers at the melt temperature of Se (~220°C), as well as the lack of solvents for solution precipitation. The polymer network was denoted as PSe_xG_y, by copolymerizing a selenium-containing monomer, bis(4-hydroxybutyl)-3,3′-selenodipropanoate (SeC2CO), which incorporates the β-selenocarbonyl structure, with polyethylene glycol (PEG, M_n = 1000) as a chain extender, glycerol as a crosslinker and equivalent stoichiometric isocyanates (Figure S1 and Table S1). Under basic and air conditions, β-selenocarbonyl unit in SeC2O underwent a coupled reaction comprising a retro-Michael elimination and subsequent oxidation by oxygen, yielding elemental selenium and corresponding α, β-unsaturated carbonyl, as confirmed by x-ray photoelectron spectroscopy (XPS) and ^{1}H-NMR (Figures 1b and S2–S4). Additionally, we incorporated a photo-base generator, 1,8-diazabicyclo[5.4.0]undec-7-ene-1-ium 2-(3-benzoylphenyl)propanoate (PBG, w = 3%) for controlling selenium formation. Upon 365 nm irradiation, the PBG could undergo UV-initiated photochemical reactions and release the organic base 1,8-diazabicyclo[5.4.0]undec-7-ene (DBU), while remaining inert prior to irradiation (Figures S5, S6). In the ^{1}H-NMR spectra, those peaks of chemical shift around 6.1 ppm, corresponding to an alkene structure, emerged in a mixture of DBU and SeC2CO, consistent with a base-triggered retro-Michael elimination (Figure S4). However, those peaks referring to alkene structures were in absence when only mixing PBG and SeC2O without irradiation, and increased after UV exposure. (Figures 1c and S7–S10). These results demonstrated controllable onset of selenium formation, thereby suppressing premature selenium generation before complete network formation, and ensuring a uniform mechanic environment for crystal growth.

After UV exposure and maintaining PSe_xG_y at 60°C, one far below the melting point of selenium (~220°C), allowed formed elemental selenium to gradually crystallize within the polymer (Figure 1d and Movie S1), forming branched crystals with an average diameter of 250 μm (Figures 1e,S11, and S12). Owing to the strong attenuation of x-rays by selenium near its K-edge and the resulting contrast relative to the polymer matrix, selenium crystals exhibit markedly lower transmittance than the surrounding polymer. This contrast enables x-ray microscopy to resolve the three-dimensional crystal morphology (red) and its spatial distribution within the polymer matrix (gray) (Figures 1a,S13). The selenium crystals form a branched morphology that expands in three dimensions. Scanning electron microscopy (SEM) revealed that they differed from conventional spherulites formed from the melt, which typically contain non-crystalline regions between radial branches. They have polymer matrix continuously filling the spaces between individual branches (Figure 1f). We proposed that this interpenetrating structure ensures intimate contact between the polymer and the advancing growth front [42], facilitating polymer-crystal interactions.

Selenium's dynamic covalent backbone is the basis for its potential dynamicity. In x-ray diffraction spectrum, although the broad background from the amorphous polymer matrix partially obscured the selenium diffraction peaks (Figure S14), they could still be indexed to the standard pattern of trigonal selenium, the most stable allotrope, in which atoms are linked by Se-Se bonds into long helical chains. (Figure 1g,h). Additionally, Raman spectroscopy could avoid signal interference from polymer (Figure S15), and identify a characteristic signal at a wavenumber of 237 cm^{-1}, corresponding to the stretching vibration of Se—Se bond within Se_n chains [43] (Figure 1i). Time-resolved in situ Raman spectra revealed the presence of amorphous selenium (a-Se, ~251 cm^{-1}) at the onset of crystallization and its rapid conversion to trigonal selenium (t-Se) via reversible Se—Se bond cleavage and reformation, suggesting that a-Se serves as a short-lived intermediate during early nucleation and growth, whereas the subsequent branching stage is dominated by t-Se (Figure S16). Mapping signal of this wavenumber precisely overlapped with the optical image of crystal (Figures 1i and S17), supporting that Se_n chain is predominant structural unit. We suggested that this specific polymer-like structure constituted by abundant Se—Se bonds introduce the susceptibility of structural perturbation into selenium crystal, particularly embodied in the interaction

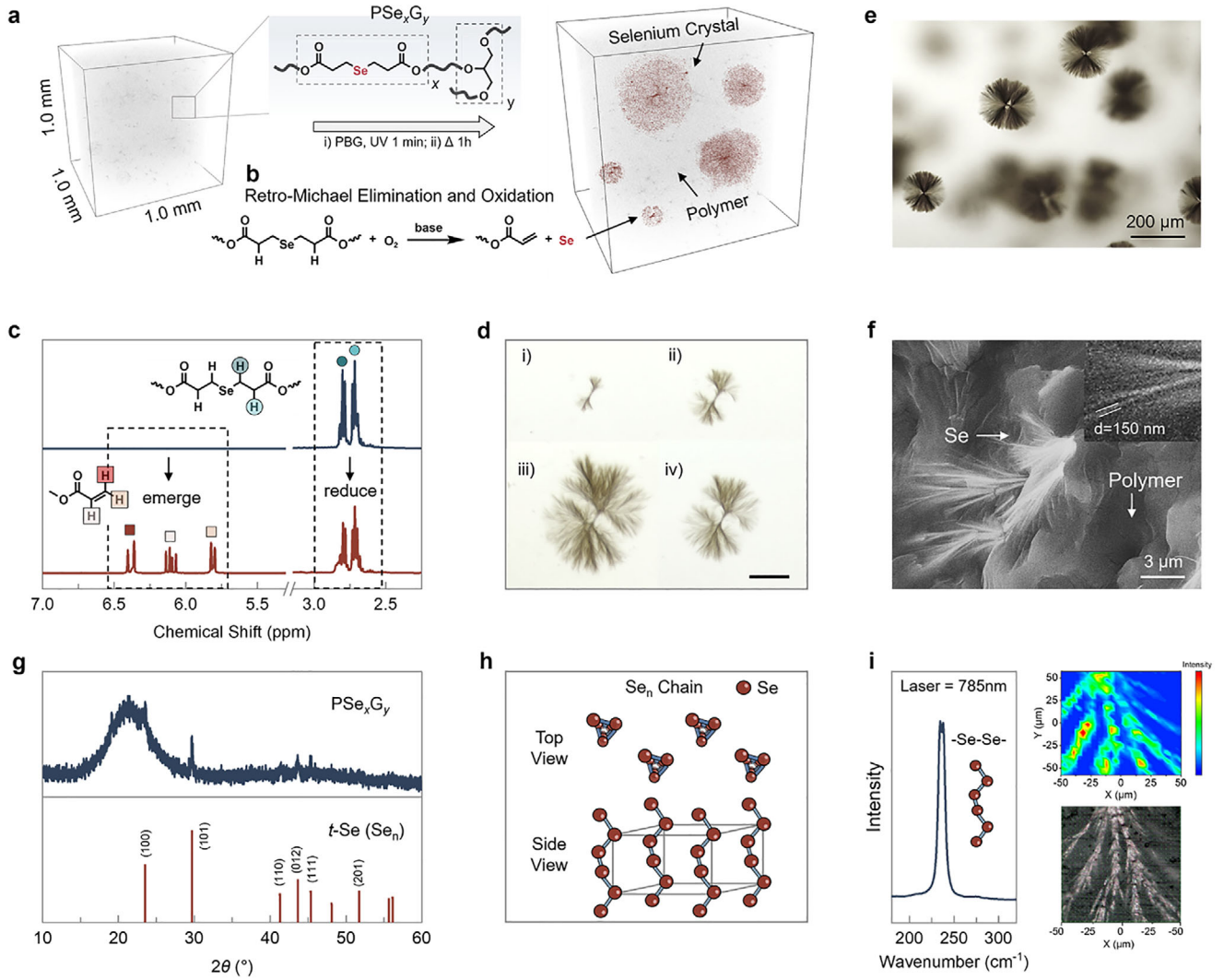

FIGURE 1 | In situ formation of selenium crystals in polymer networks (a) Schematic process of in situ reaction induced crystallization and also 3D image under x-ray microscope, where gray background refers to selenium-containing polymer (PSe_xG_y) and red part refers to selenium crystal, respectively, where x and y represent selenium monomer and crosslinker content, x (or y) = $m_{(Monomer/crosslinker)}/m_{(PEG)} \times 100\%$. (b) Coupled retro-michael reaction (elimination) and oxidation reaction. (c) ^{1}H-NMR spectrum of the mixture of SeC2O and PBG before and after UV 365 nm exposure, then heating in the air for 1 h ($CDCl_3$, 400 MHz). (d) Images of in situ growth of selenium crystal obtained by optical microscope, dark branch structure refers to selenium crystal and light part refers to polymer matrix, respectively, scale bar = 50 μm. (e) Image of branched selenium crystals within polymer network. (f) SEM image of selenium crystal within polymer matrix, scale bar = 3 μm. The thickness of branch individual is approximate 150 nm. (g) XRD spectrums of selenium crystals within polymer and standard card. (h) According selenium chains in the unit cell. (i) Raman spectrum of selenium crystals and mapping result using the wavenumber at 237 cm^{-1}, laser = 785 nm. Top figure is signal distribution and bottom one is the photograph of practical crystal.

between crystal's advancing front and polymer matrix, hopefully leading to structure response of selenium crystals under stress.

2.2 | Programable Mechanical Inputs and Adaptive Mechanical Response of Se

Conventional crystal growth methods, such as melt quenching or solution precipitation, provide limited control over local stress and thus obscuring stress-structure coupling. By contrast, our in situ growth system used polymer as a real-time, programable source of stress. Conceptionally, those polymer chains constraining the growing crystals were progressively strained, exerting stress on growth front [44] (Figure 2a). The stress magnitude was primarily governed by the mechanical property of polymer. Because crystal growth is dynamic and conducted at 60°C, one well above the glass transition temperature (T_g = −50.7 to −26.3°C) of PSe_xG_y (Figure S18), the viscoelastic response of the polymer must be carefully considered. Specifically, polymer stress depends on deformation frequency, which in this system is dictated by the crystal growth rate. At high growth rates, limited relaxation time increases stress, whereas at very low growth rates, extensive chain relaxation suppresses effective stress generation. Thus, the stress experienced by the crystal depends not only on intrinsic polymer mechanics but also on the growth rate.

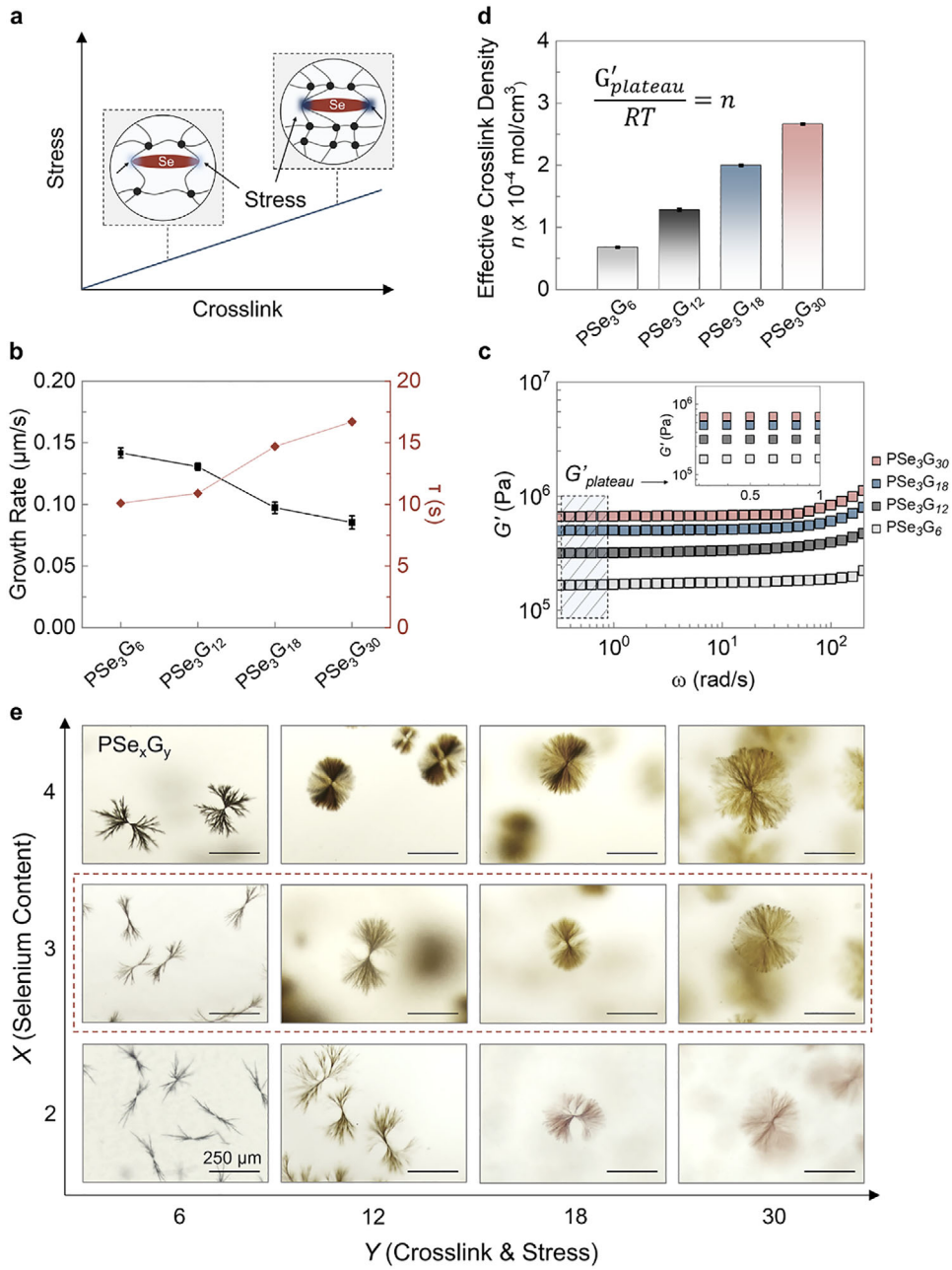

FIGURE 2 | Programable mechanical inputs and mechanical response of Se (a) Schematic process of selenium experiencing the stress exerted by polymer chains during growth. (b) Growth rate of selenium crystal within PSe_3G_y, $y = 6, 12, 18, 30$. (c) Storage moduli (G') and (d) correspondingly calculated effective crosslink density (n) of PSe_3G_y, $y = 6, 12, 18, 30$. (e) Images of selenium crystals within PSe_xG_y, $x = 2, 3, 4$ and $y = 6, 12, 18, 30$, scale bar = 250 μm.

The growth rates of selenium crystals in $PSe_3G_{y,\ y=6,\ 12,\ 18,\ 30}$ decreased slightly with increasing y, ranging from 0.14 to 0.08 μm/s, corresponding to characteristic timescales (τ) of 10.1 – 16.7 s (Figures 2b and S19). Notably, within τ this range, the polymer exhibits rate-independent elastic behavior: their storage modulus all reside on a plateau across the corresponding frequency window ($\sim 2\pi/\tau$ = 0.3–0.7 rad/s; Figures 2c,S20, and S21). Consequently, growth-rate effects can be excluded. Effective density (n) deviated from $G'_{plateau}$ can be utilized to quantify applied stress based on classical rubber elasticity [45].

$$n = \frac{G'}{RT}$$

The calculated n was 0.68×10^{-4}mol/cm^3 for PSe_3G_6 and 2.67×10^{-4}mol/cm^3 for PSe_3G_{30}, increasing with the y values (Figure 2d). Notably, these values were significantly lower that measured by low-field ^{1}H-NMR, due to the latter accounts for all crosslinks, while former only reflects stress-bearing ones (Figures S22, S23). Moreover, the rheological strain-sweep tests at 0.1 Hz show a plateau in G' for strains <1%, indicating that the network also

demonstrates a linear elastic response at this regime (Figure S24). Considering the pre-branching growth distance between two branch points is ~3 μm from SEM, which gives a nominal strain of <1% relative to the millimeter-scale matrix size, the local (microscopic) stress per unit strain accumulated in the polymer network was approximately proportional to n, obeying following equation:

$$\sigma_u \approx E \times K_t = 2(1+\gamma) nRTK_t$$

where the σ_u is the effective stress per unit strain, E is the elastic modulus of polymer, γ is the Poisson's ratio of polymer, R is the ideal gas constant, T is the temperature and K_t is the Inglis stress-concentration factor associated with the thin morphology of growth front. This framework enables a quantitative estimation of σ from experimentally measured n, demonstrating that higher effective crosslink density leads to greater stress (Figure 2a).

Having established a quantitative framework for stress evaluation, we next investigated how selenium crystals respond to mechanical signals. Twelve samples (PSe_xG_y, x = 2, 3, 4; y = 6, 12, 18, 30) were analyzed by optical microscopy (Figure 2e). Across all compositions, selenium crystals exhibited stress-adaptive architectures. At same selenium contents x, lightly crosslinked polymers produced needle-like crystals with few branches, whereas higher crosslink (y) yielded rounder morphologies with dense branching. This trend was consistent across all samples, revealing a general rule: increasing crosslink density, and thus stress promotes branching. In highly crosslinked samples, selenium crystals even displayed pronounced birefringence under polarized light, characteristic of spherulitic structures and indicative of highly frequent branch (Figure S25). At fixed crosslink density, increasing x further enhanced branching, which we attribute to a higher crystallization driving force resulting from increased precursor concentration and accelerated growth rates. These observations allow us to partially rule out diffusion as the primary origin in our system, although diffusion is often invoked to explain branched morphology. In diffusion-dominated growth, slower diffusion favors branching. In our system, increasing crosslink density does reduce internal diffusion, as confirmed by fluorescence recovery after photobleaching (FRAP) [46] (Figures S26, S27). If branching were diffusion-controlled, then at fixed crosslink density, a higher monomer concentration should suppress branching by enhancing the local diffusion rate of selenium species to the growth front. Instead, we observe the opposite trend: increasing the selenium-containing monomer content markedly enhances branching (Figure S28). This contradiction indicates that branch formation bases predominantly on a mechanical stress-adaptive mode rather than diffusion-controlled one.

2.3 | Adaptive Branching Modes in Selenium Crystals

To further verify the dynamic branching mode of selenium crystals, we developed an integrated framework combining mathematical modeling, deep learning, and experimental imaging (Figure 3a, Supporting Information). First, we established a quantitative link between microscopic branching and macroscopic morphology using a stochastic 3D growth model based on Markov process [47, 48] (Figures 3a, and S29). This model simulated the continuous forward growth of crystal tips with stochastic directional deviations and reveals a positive correlation between branching frequency f and morphological isotropy: increasing f yields rounder, more spherical structures (Figure S30). These simulated morphologies exhibited strong agreement with experimental selenium crystal images obtained under different stress conditions, validating the simulation's physical relevance. And then, we further developed a deep learning-based framework ResNet34 [49–51] to invert the distribution of f from experimental 2D projection images (Supporting Information). Although indirect, this approach offers two advantages: (1) Resolution Independence: It bypasses the optical resolution limit by inferring microscopic branching generations from macroscopic morphological descriptors (e.g., anisotropy and fractal dimension, Figure S31 and Table S2), eliminating manual counting errors associated with blurred boundaries. (2) Orientation Invariance: It decouples morphological features from observation angles. Since experimental micrographs are 2D projections of randomly oriented 3D crystals, our model is trained on a dataset comprising projections of simulated models from exhaustive viewpoints (Figure S32), enabling robust prediction regardless of the crystal's orientation (Figures S33, S34). Applying this framework, we identified a stress-adaptive branching mechanism in selenium crystals: an increase in crosslink density, that is stress magnitude drives a corresponding increase in branching frequency (Figure 3b,c), facilitating a structure evolution from needle to sphere. (Figure 3d).

2.4 | Mechanistic Origin of Se—Se Bond-Mediated Mechanic and Light Responsiveness

We propose that the dynamic behavior of selenium crystals originated from the responsiveness of Se—Se bonds. In our previous work, we demonstrated that Se—Se bonds enable efficient stress relaxation in polymer materials via Se—Se exchange-mediated network reconstruction [36]. In analogy, we posit that stress relaxation at growth fronts, driven by force-induced Se—Se cleavage and reformation, underlies the stress-adaptive branching of selenium crystals. Figure 4a qualitatively illustrates the relationship between local stress accumulation and the growth/branching behavior of an individual crystal branch. As the crystal grows in an elastic medium, stress (σ) progressively accumulates at the advancing front with propagation distance (d). When the local stress approaches a critical level sufficient to activate Se—Se exchange, the structural order of the Se_n chains can consequently be disrupted, generating dislocations or defects. These localized structural deformations promote stress relaxation [52]. Simultaneously, they act as nucleation sites that cause newly formed sub-individuals to deviate from the orientation of the parent crystal, ultimately giving rise to macroscopic branches [53]. From an energy perspective, crystal propagation in an elastic matrix progressively accumulates elastic strain energy, and branching becomes thermodynamically favorable when the reduction of elastic energy outweighs the cost of creating additional interfaces that lead to branching [54, 55]. Here, the critical stress (σ_c) for Se—Se exchange is treated as an effective phenomenological threshold, and the relationship between elastic modulus (E) and d does not rely on its exact value. Assuming that the

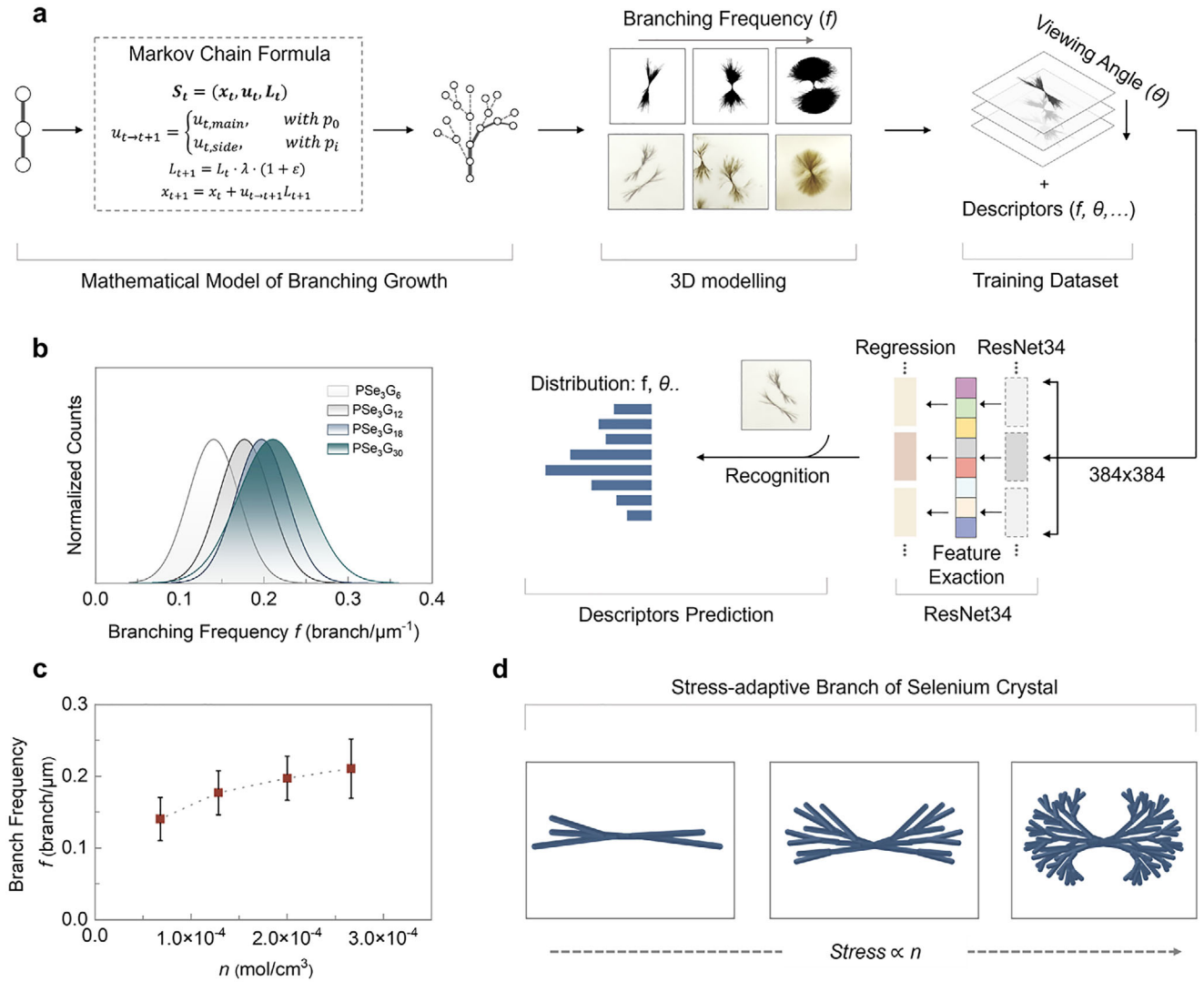

FIGURE 3 | Adaptive branching modes in selenium crystals (a) Schematic process of 3D modelling of branched structure and deep learning-assistant image recognition for inverting structural descriptors of branched crystals. x_t is the tip position, u_t is the branch orientation, ℓ_t is the advancing length, p is probability, s represents the state, λ represents the length decay factor, and ε stands for the perturbation of length. (b) Distribution of branch frequency of PSe_3G_y, $y = 6, 12, 18, 30$. (c) The relationship between branch frequency of PSe_3G_y and effective crosslink density n. (d) Adaptive mode of selenium crystals to stress.

accumulated strain (ε) scales with the propagation distance (d), the local stress follows the linear elastic relation: $\sigma \propto E\varepsilon$, giving $\sigma \propto Ed$. The characteristic branching interval (d_c) is expected to scale inversely with the matrix modulus, that is $d_c \propto E^{-1}$. Accordingly, the branching frequency (f) follows $f \propto 1/d_c \propto E \propto n$. This mechanism, based on Se—Se bond-mechanics coupling, implies a general rule for branch regulation: a stiffer matrix requires a shorter propagation distance to reach the effective stress level for Se—Se exchange, thereby increasing the branching frequency (Figure 4b).

Based on our understanding that Se—Se exchange governs the dynamic branching behavior of selenium crystals under mechanical stimulation, this responsiveness can be rationally extended beyond mechanical fields. Since Se—Se bond are photo-responsive and can undergo exchange upon light irradiation, light may provide an orthogonal means to dynamically regulate branching during growth (Figure 4c). In our system, mechanical forces are geometrically related and opposite to the local advancing direction, which is crucial for inducing branching. In contrast, light does not have such a strict physical relation to the growth direction. Consequently, photoinduced Se—Se exchange is expected to occur more uniformly in space, without inducing macroscopic branching along specific orientations. Instead, such bond rearrangement would lead to averaged microscopic structural reorganization, which macroscopically manifests as additional stress relaxation at the growth front, leading to suppressed macroscopic branching (Figure 4d). Our experimental results are consistent with this expectation: the branching frequency in the illuminated group is significantly lower than that in the non-illuminated controls (Figure 4e,f). Even under high-power irradiation, only very small crystals can be observed under a microscope (Figure S35) which we attributed to excessive Se—Se exchange that disrupts the long-range ordering of selenium chains, and impedes the growth of large crystals [56]. Once removing the irradiation, those small crystals serve as

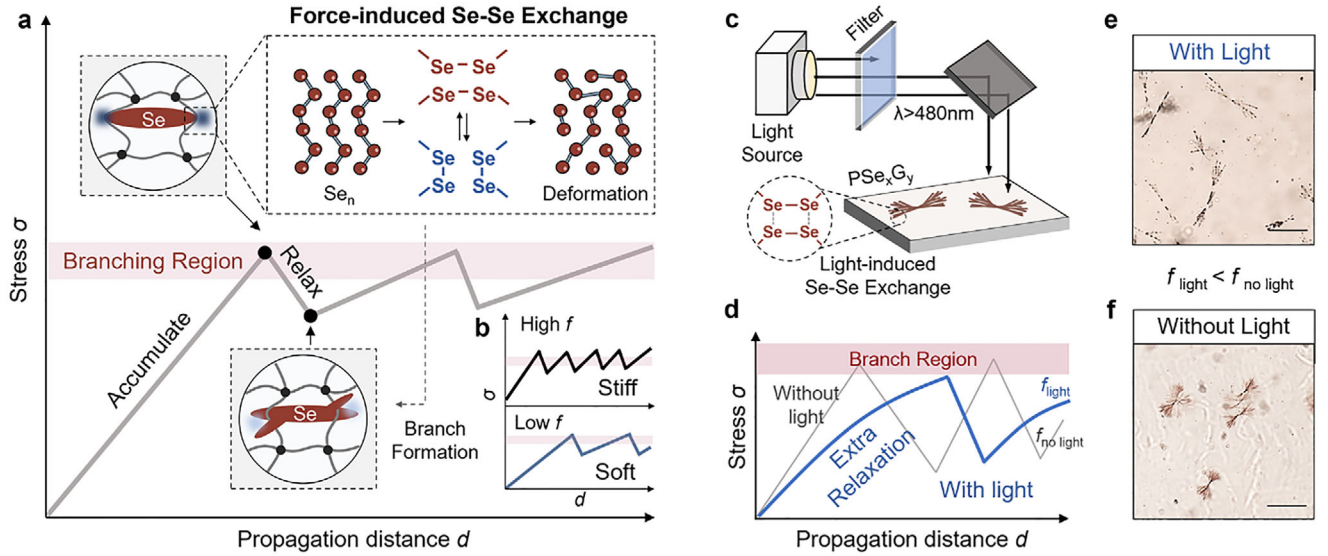

FIGURE 4 | Mechanistic origin of Se—Se bond-mediated mechanic and light responsiveness (a) Schematic mechanism of branch formation through force-induced Se—Se exchange and changes in magnitude of system's total stress, involving stress accumulation, relaxation. Branching region represents a stress window near Se—Se effective activation condition. (b) Comparison of branch frequency *f* of crystals within soft and stiff polymer matrices. (c) The process of introducing light in real time during growth. The light source is Xe lamp, power = 2 W. (d) Mechanism of light responsiveness of selenium crystals. (e, f) Images of crystals within PSe_3G_{12} growing with and without light, scale bar = 250 μm.

nuclei, enabling the subsequent regrowth of observable branched crystals (Figure S36). Collectively, these results strongly support a chemo-mechanical coupling mechanism, whereby the dynamic response of selenium crystals arises from bond-level Se—Se exchange rather than from purely mechanical effects.

2.5 | Tunable Dielectric Behavior in Polymer-Selenium Composites

Beyond architectural control, the properties of selenium crystals can also be modulated within our crystal-polymer composite system. During in situ crystallization, PSe_xG_y evolves from a pure polymer into a composite in which selenium crystals are embedded in the matrix and function as inorganic fillers. Those crystals effectively reinforce the matrix and enhance the overall mechanical strength (Figure S37). In addition, as a typical semiconductor, selenium substantially modifies the dielectric behavior of the host polymer. Previous studies have established that the morphology of inorganic fillers critically determines the magnitude of dielectric enhancement: fillers with high aspect ratios concentrate electric fields at tips and readily to reach percolation threshold, producing a pronounced increase in the effective dielectric constant (ε') [57, 58] (Figure 5a). In our system, selenium crystals exhibit programable aspect ratios through stress-adaptive branching growth, providing a direct route to on-demand tuning of dielectric properties.

Prior to in situ crystal growth, the ε' of the PSe_3G_y was approximately 30, decreasing slightly as *y* increased, likely due to reduced chain mobility and suppressed polarization under an electric field. Notably, selenium monomers facilitated the polarity of polymer networks, resulting in a higher ε' than those without selenium monomers (Figure S38). After in situ growth of selenium crystals, the dielectric constant increased markedly (e.g., from 28.2 to 50.9 in sample PSe_3G_6) (Figures 5b and S39). To exclude the effect of PBG, we measured materials with varying PBG content and without crystals. Although their ε' increased with higher PBG content, they remained significantly lower than those of materials with selenium crystals (Figure S40). This confirms that selenium crystals primarily contribute to the increased dielectric constant. Furthermore, the crystal morphology is critical for dielectric enhancement. Needle-like crystals with fewer branches provide the greatest increase in dielectric constant. As branching increases and crystals become more spherical, the enhancement diminishes. (Figure 5b). Furthermore, we physically doped an equivalent amount of spherical selenium powder into polymer and observed only a slight increase in dielectric constant, comparable to the most highly branched, spherical crystal samples (Figures 5c and S41). This supports the conclusion that enhancements are indeed morphology-dependent. Consequently, selenium crystal is a functional inorganic material beyond a filler, by mechanically programing selenium crystal branching, we can produce composite materials with tunable dielectric properties, demonstrating a multi-scale and dynamic regulation of selenium crystal from its structure to performance.

3 | Conclusion

In this work, we experimentally demonstrate the availability of endowing responsiveness into inorganic crystals through dynamic covalent bond and regulating their structures and properties by external stimuli. Using elemental selenium as a model system and polymer as growth matrix, we overcome the limitation arising in part from the absence of intrinsic bond-level dynamicity in typical inorganic solids, as well as from the lack of a growth environment capable of exerting real-time, persistent, and microscopically relevant regulation. Although direct, in situ visualization of Se—Se bond cleavage and reformation at the growth front remains experimentally challenging, the

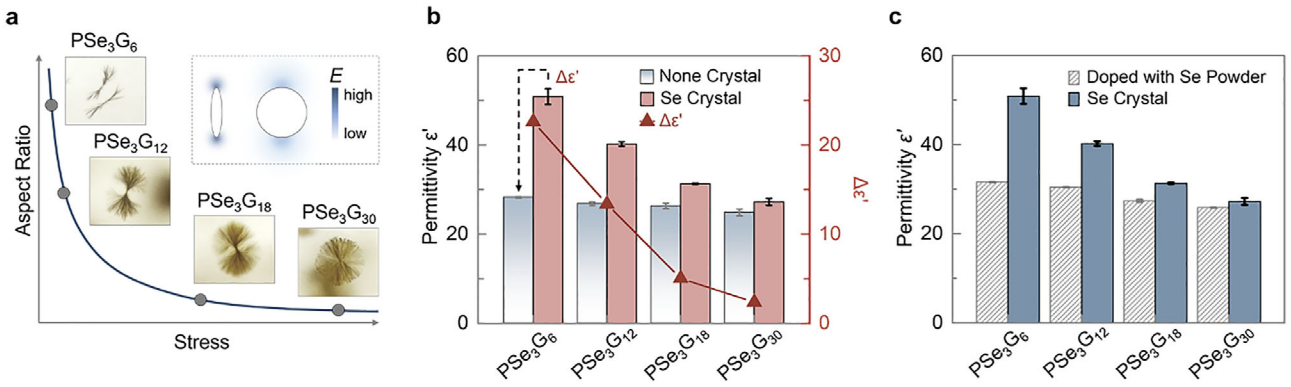

FIGURE 5 | Tunable dielectric behavior in polymer-selenium composites (a) Schematic relationship between aspect ratio of selenium crystals and strength of deformation in electric field. (b) Dielectric constant of PSe_3G_y ($y = 6, 12, 18, 30$) before and after growing selenium crystals, f = 1 kHz. (c) Comparison of ε' of PSe_3G_y ($y = 6, 12, 18, 30$) after growing Se crystals and physically doped with spherical Se powder at same content, f = 1 kHz.

consistent correlation between regulation by mechanic stress and light irradiation, crystal architecture, and functional dielectric response provides strong evidence that bond-level dynamics are operative within the crystal lattice. We provide an inspiring, interdisciplinary research paradigm to bridge the dynamic covalent chemistry and inorganic materials. This paradigm can be extended to uncover more adaptive inorganic materials, such as chalcogen compounds containing disulfide, diselenide, or ditelluride bonds. Furthermore, the synergy between a programmable matrix and intrinsic dynamicity may offers a new perspective on biomineralization, inspiring how nature regulates the growth of complex, hierarchical structures through dynamic interfacial constraints.

Author Contributions

Chaowei He: conceptualization, validation, software, methodology, formal analysis, data curation, writing - original draft, investigation. **Wenjie Zhang:** methodology, software, data curation, formal analysis, writing - original draft, investigation. **Ruihao Zhou:** formal analysis. **Zeyu Lu:** formal analysis. **Zhigang Shuai:** investigation, writing - review and editing. **Huaping Xu:** supervision, conceptualization, funding acquisition, writing - review and editing.

Acknowledgments

This work was financially supported by the National Natural Science Foundation of China (52233012, 22025302), the XPLORE PRIZE, and the Beijing Outstanding Young Scientist Program. We thank Prof. Liang Zhang (Tsinghua University) for his suggestions on Raman analysis and Prof. Jun Guan for her suggestions on manuscript writing. We thank Dr. Xiaobin Dai for his suggestions on mathematical modelling. We also thank Jingjing Wang at Cell Biology Facility, Center of Biomedical Analysis, Tsinghua University for the technical support and assistance with confocal imaging experiments.

Conflicts of Interest

The authors declare no conflicts of interest.

Data Availability Statement

The data that support the findings of this study are available on request from the corresponding author. The data are not publicly available due to privacy or ethical restrictions.

References

1. L. Montero de Espinosa, W. Meesorn, D. Moatsou, and C. Weder, "Bioinspired Polymer Systems With Stimuli-Responsive Mechanical Properties," *Chemical Reviews* 117 (2017): 12851–12892, https://doi.org/10.1021/acs.chemrev.7b00168.

2. A. Lendlein and O. E. C. Gould, "Reprogrammable Recovery and Actuation Behaviour of Shape-Memory Polymers," *Nature Reviews Materials* 4 (2019): 116–133, https://doi.org/10.1038/s41578-018-0078-8.

3. T. Matsuda, R. Kawakami, R. Namba, T. Nakajima, and J. P. Gong, "Mechanoresponsive Self-growing Hydrogels Inspired by Muscle Training," *Science* 363 (2019): 504–508, https://doi.org/10.1126/science.aau9533.

4. C. Liu, C. He, X. Dai, L.-T. Yan, and H. Xu, "Achieving Mechanical Evolution in Polymer Materials Through Phase Evolution Induced by Visible Light," *Advanced Materials* 37 (2025): e08549, https://doi.org/10.1002/adma.202508549.

5. O. Sato, "Dynamic Molecular Crystals With Switchable Physical Properties," *Nature Chemistry* 8 (2016): 644–656, https://doi.org/10.1038/nchem.2547.

6. P. Naumov, S. Chizhik, M. K. Panda, N. K. Nath, and E. Boldyreva, "Mechanically Responsive Molecular Crystals," *Chemical Reviews* 115 (2015): 12440–12490, https://doi.org/10.1021/acs.chemrev.5b00398.

7. P. Naumov, D. P. Karothu, E. Ahmed, et al., "The Rise of the Dynamic Crystals," *Journal of the American Chemical Society* 142 (2020): 13256–13272, https://doi.org/10.1021/jacs.0c05440.

8. L. Lan and H. Zhang, "Maneuverability and Processability of Molecular Crystals," *Angewandte Chemie International Edition* 63 (2024): e202411405, https://doi.org/10.1002/anie.202411405.

9. I. Tahir, E. Ahmed, D. P. Karothu, F. Fsehaye, J. Mahmoud Halabi, and P. Naumov, "Photomechanical Crystals as Light-Activated Organic Soft Microrobots," *Journal of the American Chemical Society* 146 (2024): 30174–30182, https://doi.org/10.1021/jacs.4c08320.

10. C. Ding, B. Tang, Y. Zhou, et al., "Cryogenically Self-healing Organic Crystals," *Nature Materials* 25 (2025): 285–293.

11. S. Maes, N. Badi, J. M. Winne, and F. E. Du Prez, "Taking Dynamic Covalent Chemistry Out of the Lab and Into Reprocessable Industrial Thermosets," *Nature Reviews Chemistry* 9 (2025): 144–158, https://doi.org/10.1038/s41570-025-00686-7.

12. Z. Lei, H. Chen, S. Huang, L. J. Wayment, Q. Xu, and W. Zhang, "New Advances in Covalent Network Polymers via Dynamic Covalent Chemistry," *Chemical Reviews* 124 (2024): 7829–7906, https://doi.org/10.1021/acs.chemrev.3c00926.

13. N. R. Boynton, J. M. Dennis, N. D. Dolinski, et al., "Accessing Pluripotent Materials Through Tempering of Dynamic Covalent Polymer

Networks," *Science* 383 (2024): 545–551, https://doi.org/10.1126/science.adi5009.

14. S. J. Rowan, S. J. Cantrill, G. R. L. Cousins, J. K. M. Sanders, and J. F. Stoddart, "Dynamic Covalent Chemistry," *Angewandte Chemie International Edition* 41 (2002): 898–952, https://doi.org/10.1002/1521-3773(20020315)41:6%3c898::AID-ANIE898%3e3.0.CO;2-E.

15. M. Hua, Z. Peng, R. D. Guha, et al., "Mechanochemically Accelerated Deconstruction of Chemically Recyclable Plastics," *Science Advances* 10 (2024): eadq3801, https://doi.org/10.1126/sciadv.adq3801.

16. M. Podgórski, B. D. Fairbanks, B. E. Kirkpatrick, et al., "Toward Stimuli-Responsive Dynamic Thermosets Through Continuous Development and Improvements in Covalent Adaptable Networks (CANs)," *Advanced Materials* 32 (2020): 1906876, https://doi.org/10.1002/adma.201906876.

17. Q.-H. Guo, M. Jia, Z. Liu, et al., "Single-Crystal Polycationic Polymers Obtained by Single-Crystal-to-Single-Crystal Photopolymerization," *Journal of the American Chemical Society* 142 (2020): 6180–6187, https://doi.org/10.1021/jacs.9b13790.

18. Y. Deng, L. Liu, H.-X. Luo, et al., "Supramolecular Chemical Recycling of Dynamic Polymers," *Nature Nanotechnology* 20 (2025): 1805–1812, https://doi.org/10.1038/s41565-025-02041-9.

19. Z.-B. Zhu, X. Li, L. Liu, et al., "Single-Crystalline Poly(disulfide)s Enabled by PhotoTriggered Topochemical Ring-Opening Polymerization of 1,2-Dithiolane," *Journal of the American Chemical Society* 147 (2025): 42743.

20. Q. Xu, X. Wang, S. Huang, et al., "Dynamic Covalent Self-Sorting in Molecular and Polymeric Architectures Enabled by Spiroborate Bond Exchange," *Angewandte Chemie International Edition* 62 (2023): e202304279, https://doi.org/10.1002/anie.202304279.

21. W. M. Awad, D. W. Davies, D. Kitagawa, et al., "Mechanical Properties and Peculiarities of Molecular Crystals," *Chemical Society Reviews* 52 (2023): 3098–3169, https://doi.org/10.1039/D2CS00481J.

22. S. Hasebe, Y. Hagiwara, T. Asahi, and H. Koshima, "Actuation Performance and Versatility of Photothermally Driven Organic Crystals," *Angewandte Chemie International Edition* 64 (2025): e202418570, https://doi.org/10.1002/anie.202418570.

23. N. K. Nath, L. Pejov, S. M. Nichols, et al., "Model for Photoinduced Bending of Slender Molecular Crystals," *Journal of the American Chemical Society* 136 (2014): 2757–2766, https://doi.org/10.1021/ja4101497.

24. X.-D. Qiu, L. Chen, J.-W. Hou, et al., "Regulating Reversible Untwisting and Twisting Motions in Helical Dynamic Molecular Crystals," *Journal of the American Chemical Society* 147 (2025): 17772–17783, https://doi.org/10.1021/jacs.5c01145.

25. S. Kobatake, S. Takami, H. Muto, T. Ishikawa, and M. Irie, "Rapid and Reversible Shape Changes of Molecular Crystals on Photoirradiation," *Nature* 446 (2007): 778–781, https://doi.org/10.1038/nature05669.

26. R. Boyd, "Selenium Stories," *Nature Chemistry* 3 (2011): 570, https://doi.org/10.1038/nchem.1076.

27. M. Zhu, G. Niu, and J. Tang, "Elemental Se: Fundamentals and Its Optoelectronic Applications," *Journal of Materials Chemistry C* 7 (2019): 2199–2206, https://doi.org/10.1039/C8TC05873C.

28. M. C. Coughlin and B. Wunderlich, "Extended-Chain Crystals. VII. Lamellar and Fibrillar Spherulites in Selenium," *Journal of Polymer Science Part B: Polymer Letters* 10 (1972): 57–61, https://doi.org/10.1002/pol.1972.110100110.

29. B. Yan, X. Liu, W. Lu, et al., "Indoor Photovoltaics Awaken the World's First Solar Cells," *Science Advances* 8: eadc9923, https://doi.org/10.1126/sciadv.adc9923.

30. R. G. Crystal, "The Polymeric Nature of Selenium Crystallization. I. Morphology and Thermodynamic Considerations," *Journal of Polymer Science Part A-2: Polymer Physics* 8 (1970): 1755–1772, https://doi.org/10.1002/pol.1970.160081011.

31. F. Fan, S. Ji, C. Sun, et al., "Wavelength-Controlled Dynamic Metathesis: A Light-Driven Exchange Reaction Between Disulfide and Diselenide Bonds," *Angewandte Chemie International Edition* 57 (2018): 16426–16430, https://doi.org/10.1002/anie.201810297.

32. S. Ji, W. Cao, Y. Yu, and H. Xu, "Dynamic Diselenide Bonds: Exchange Reaction Induced by Visible Light Without Catalysis," *Angewandte Chemie International Edition* 53 (2014): 6781–6785, https://doi.org/10.1002/anie.201403442.

33. J. Xia, P. Zhao, S. Pan, and H. Xu, "Diselenide-Containing Polymeric Vesicles With Osmotic Pressure Response," *ACS Macro Letters* 8 (2019): 629–633, https://doi.org/10.1021/acsmacrolett.9b00250.

34. X. Li, F. Yang, Y. Li, et al., "Diselenide as a Dual Functional Mechanophore Capable of Stress Self-Reporting and Self-Strengthening in Polyurethane Elastomers," *CCS Chemistry* 5 (2022): 925–933, https://doi.org/10.31635/ccschem.022.202201874.

35. C. Liu, Z. Fan, Y. Tan, F. Fan, and H. Xu, "Tunable Structural Color Patterns Based on the Visible-Light-Responsive Dynamic Diselenide Metathesis," *Advanced Materials* 32 (2020): 1907569, https://doi.org/10.1002/adma.201907569.

36. Y. Tan and H. Xu, "Selenium-Containing Dynamic Materials: Structure Programming Through Selective Dissipation," *Accounts of Materials Research* 5 (2024): 739–751, https://doi.org/10.1021/accountsmr.4c00065.

37. R. G. Crystal, "Polymeric Nature of Selenium Crystallization. II. Crystallization Kinetics and Secondary Crystallization," *Journal of Polymer Science Part A-2: Polymer Physics* 8 (1970): 2153–2161, https://doi.org/10.1002/pol.1970.160081211.

38. W. Lu, Z. Li, M. Feng, et al., "Structure of Amorphous Selenium: Small Ring, Big Controversy," *Journal of the American Chemical Society* 146 (2024): 6345–6351, https://doi.org/10.1021/jacs.4c00219.

39. X. Wen, Z. Li, W. Lu, et al., "Illumination-assisted Annealing Enables Selenium Solar Cells With Open-circuit Voltage Over 1 V and Efficiency Exceeding 10%," *Nature Energy* 11 (2026): 274–283, https://doi.org/10.1038/s41560-025-01939-x.

40. A. V. Kolobov, H. Oyanagi, K. Tanaka, and K. Tanaka, "Structural Study of Amorphous Selenium by in Situ EXAFS: Observation of Photoinduced Bond Alternation," *Physical Review B* 55 (1997): 726–734, https://doi.org/10.1103/PhysRevB.55.726.

41. V. V. Poborchii, A. V. Kolobov, and K. Tanaka, "An In Situ Raman Study of Polarization-dependent Photocrystallization in Amorphous Selenium Films," *Applied Physics Letters* 72 (1998): 1167–1169, https://doi.org/10.1063/1.121002.

42. H. Li, H. L. Xin, D. A. Muller, and L. A. Estroff, "Visualizing the 3D Internal Structure of Calcite Single Crystals Grown in Agarose Hydrogels," *Science* 326 (2009): 1244–1247, https://doi.org/10.1126/science.1178583.

43. G. Lucovsky, A. Mooradian, W. Taylor, G. B. Wright, and R. C. Keezer, "Identification of the Fundamental Vibrational Modes of Trigonal, α—Monoclinic and Amorphous Selenium," *Solid State Communications* 5 (1967): 113–117, https://doi.org/10.1016/0038-1098(67)90006-3.

44. D. Palin, R. W. Style, J. Zlopaša, et al., "Forming Anisotropic Crystal Composites: Assessing the Mechanical Translation of Gel Network Anisotropy to Calcite Crystal Form," *Journal of the American Chemical Society* 143 (2021): 3439–3447, https://doi.org/10.1021/jacs.0c12326.

45. H. M. James and E. Guth, "Theory of the Elastic Properties of Rubber," *Journal of Chemical Physics* 11 (1943): 455–481, https://doi.org/10.1063/1.1723785.

46. A. Bläßle, G. Soh, T. Braun, et al., "Quantitative Diffusion Measurements Using the Open-source Software PyFRAP," *Nature Communications* 9 (2018): 1582.

47. B. Crist and J. M. Schultz, "Polymer Spherulites: A Critical Review," *Progress in Polymer Science* 56 (2016): 1–63, https://doi.org/10.1016/j.progpolymsci.2015.11.006.

48. X. Pennec, "Intrinsic Statistics on Riemannian Manifolds: Basic Tools for Geometric Measurements," *Journal of Mathematical Imaging and Vision* 25 (2006): 127–154, https://doi.org/10.1007/s10851-006-6228-4.

49. W. Xu, Y.-L. Fu, and D. Zhu, "ResNet and Its Application to Medical Image Processing: Research Progress and Challenges," *Computer Methods and Programs in Biomedicine* 240 (2023): 107660, https://doi.org/10.1016/j.cmpb.2023.107660.

50. K. He, X. Zhang, S. Ren, and J. Sun, "Deep Residual Learning for Image Recognition," in 2016 IEEE Conference on Computer Vision and Pattern Recognition (CVPR) (2016), 770–778, https://doi.org/10.1109/CVPR.2016.90.

51. D. P. Kingma, "Adam: A Method for Stochastic Optimization," arXiv preprint arXiv:1412.6980 (2014), https://arxiv.org/abs/1412.6980.

52. Y. O. Punin, "Structural and Orientational Instability of Crystals During Their Growth," *Journal of Structural Chemistry* 35 (1994): 616–624, https://doi.org/10.1007/BF02578330.

53. A. G. Shtukenberg, Y. O. Punin, E. Gunn, and B. Kahr, "Spherulites," *Chemical Reviews* 112 (2012): 1805–1838, https://doi.org/10.1021/cr200297f.

54. M. A. Grinfeld, "The Stress Driven Instability in Elastic Crystals: Mathematical Models and Physical Manifestations," *Journal of Nonlinear Science* 3 (1993): 35–83, https://doi.org/10.1007/BF02429859.

55. R. J. Asaro and W. A. Tiller, "Interface Morphology Development During Stress Corrosion Cracking: Part I. Via Surface Diffusion," *Metallurgical Transactions* 3 (1972): 1789–1796, https://doi.org/10.1007/BF02642562.

56. A. Roy, A. V. Kolobov, and K. Tanaka, "Laser-induced Suppression of Photocrystallization Rate in Amorphous Selenium Films," *Journal of Applied Physics* 83 (1998): 4951–4956, https://doi.org/10.1063/1.367296.

57. S. K. Patil, M. Y. Koledintseva, R. W. Schwartz, and W. Huebner, "Prediction of Effective Permittivity of Diphasic Dielectrics Using an Equivalent Capacitance Model," *Journal of Applied Physics* 104 (2008): 074108, https://doi.org/10.1063/1.2976173.

58. H. Tang, Z. Zhou, and H. A. Sodano, "Relationship Between $BaTiO_3$ Nanowire Aspect Ratio and the Dielectric Permittivity of Nanocomposites," *ACS Applied Materials & Interfaces* 6 (2014): 5450–5455, https://doi.org/10.1021/am405038r.

Supporting Information

Additional supporting information can be found online in the Supporting Information section.

Supporting File 1: anie72703-sup-0001-SuppMat.pdf.

Supporting File 2: anie72703-sup-0002-Movie-S1.mp4.